Available online at www.sciencedirect.com
ScienceDirect
Journal of the European Ceramic Society 30 (2010) 1287–1295
www.elsevier.com/locate/jeurceramsoc

Crystallisation behaviour and high-temperature stability of stone wool fibres

Morten M. Smedskjaer [a], Mette Solvang [b], Yuanzheng Yue [a,*]

[a] *Section of Chemistry, Aalborg University, Sohngaardsholmsvej 57, DK-9000 Aalborg, Denmark*
[b] *Rockwool International A/S, Hovedgaden 584, DK-2640 Hedehusene, Denmark*

Received 17 September 2009; received in revised form 16 November 2009; accepted 7 December 2009
Available online 6 January 2010

Abstract

The influences of the chemical composition and the heat-treatment conditions on both the crystallisation behaviour and the high-temperature stability (HTS) of three types of amorphous stone wool fibres of iron-bearing alumino-silicate composition are studied by performing thermal, structural, and compositional analyses. The fibres heat-treated under oxidising conditions exhibit outstanding HTS, i.e., the fibres are able to maintain their original geometric shape in a high-temperature environment. This is attributed to the formation of a nano-crystalline layer on the surface of the fibres as a consequence of the oxidation of Fe^{2+} to Fe^{3+}. The layer remains after the bulk crystallisation process has been completed. The thickness of the layer increases with increasing initial content of Fe^{2+} and Mg^{2+} in the fibres. The nanolayer influences the bulk crystallisation in the manner that it lowers the crystallisation onset temperature, the activation energy, and the Avrami parameter. Such influence benefits the enhancement of the HTS. In contrast, the fibres heat-treated under reducing and inert conditions exhibit poor HTS. This is attributed to the early viscous heating of the fibres because of lack of the nano-crystalline surface layer. The HTS does not depend on the identity of the bulk crystalline phases.

Keywords: Fibres; Surfaces; Thermal properties; Glass–ceramics; Oxidation

1. Introduction

Stone wool fibres (SWFs) belong to the iron-bearing alumino-silicate glass system and are used as typical heat and acoustic insulation material and fire barrier due to their excellent high-temperature stability (HTS).[1,2] A good HTS implies that the fibres are able to retain their original geometric shape at high temperatures. The HTS of SWFs results from their special crystallisation behaviour.[2] Previous investigations have shown that the HTS of the fibres strongly depends on the atmosphere in which they are heated. When the fibres are heated in an oxidising atmosphere at temperatures around 1000 °C, their shape and flexibility remain almost unchanged. However, when the fibres are heated at the same temperature in an inert or reducing atmosphere, they shrink and sinter, and hence, lose their shape and become hard and brittle.[2,3]

In most of the commercial SWF products, iron exists in the ferrous (Fe^{2+}) state due to the highly reducing condition utilised during the production of SWFs.[4,5] The ferrous ions are oxidised to ferric (Fe^{3+}) ions when SWFs are heated in atmospheric air at temperatures above $\sim 0.8T_g$ (in K), where T_g is the glass transition temperature.[4] According to previous studies,[6–12] the oxidation occurs by a diffusion process of divalent network-modifying cations towards the surface, and not a diffusion process of oxygen from the surface into the bulk of the glass. This so-called outward diffusion of divalent cations takes place to charge balance an inward flux of electron holes that move via the oxidation process of Fe^{2+} to Fe^{3+}. At the surface, the divalent cations react with the oxygen in the air, creating a nano-crystalline surface layer consisting primarily of MgO.[7,9,12] This oxidation process has a strong impact on the bulk crystallisation behaviour at temperatures well above T_g since different chemical conditions for nucleation and crystal growth are created. The formation of the nano-crystalline surface layer shifts the onset temperature of crystallisation (T_c) to a lower value.[12] The formation of the nano-crystalline surface layer has been found to be the predominant origin of the good HTS of SWFs in oxidising atmospheres. Therefore, it is possible to enhance the HTS by preoxidising (i.e., heat-treatment in air at temperatures around T_g) SWFs in atmospheric air.[3,12]

* Corresponding author. Tel.: +45 99408522; fax: +45 96350558.
E-mail address: yy@bio.aau.dk (Y. Z. Yue).

0955-2219/$ – see front matter © 2009 Elsevier Ltd. All rights reserved.
doi:10.1016/j.jeurceramsoc.2009.12.009

This work studies the influence of the chemical composition and the heat-treatment conditions on both the crystallisation behaviour and the HTS of iron-bearing alumino-silicate glass fibres. The relationship between the crystallisation behaviour and the HTS of SWFs is explored. This is done by iso-thermally treating the fibres at 1000 °C for 30 min and characterizing these fibres using the X-ray diffraction (XRD), scanning electron microscopy (SEM), and secondary neutral mass spectroscopy (SNMS) techniques. In addition, the crystallisation temperatures and activation energy are determined by recording differential scanning calorimetry (DSC) signals of the as-prepared fibres in atmospheres of air and argon. The effect of preoxidation on the crystallisation behaviour of the SWFs is also investigated.

Recently, some studies have been conducted regarding the influence of oxygen partial pressure,[3,13] redox state and amount of iron,[14–18] heat-treatment schedule,[19,20] and chemical aging[21] on the crystallisation behaviour of iron-bearing silicate glasses. However, to our knowledge, the effects of both chemical composition and heat-treatment atmosphere have not yet been investigated in the same study. Therefore, these effects are systematically investigated in this study by using various analytical techniques. This study may therefore benefit the development of new types of glass–ceramics with improved properties. Such glass–ceramics can be produced relatively inexpensively since basalt rocks are iron-bearing silicates.

2. Experimental procedure

2.1. Sample preparation and heat-treatment

The compositions of the studied glass fibres are given in Table 1. The fibre F1 has a higher content of SiO_2, Al_2O_3, and MgO than F2. F3 has a lower content of Fe^{2+} and alkaline earth oxides than F1 and F2, but contains a higher amount of alkali oxides. The fibres F1 and F2 were spun from a melt of the composition given in Table 1 using a cascade spinning process (a type of centrifuge process).[1,22] The raw materials were melted under strong reducing conditions created by burning of coke in a cupola furnace at about 1500 °C.[12] This caused a complete reduction of ferric ions in the melt to ferrous ions and free iron. The free iron was well separated and removed prior to the spinning process. The fibres were spun by pouring the melt onto the first wheel of a four wheel spinner. The melt was then transferred to adjacent wheels, where it was spun into fibres. During the spinning process, the melt was hyperquenched at a rate of $\sim 10^6$ °C/s,[23] and thereby, the ferrous state of iron in the melt is completely frozen-in in the fibres. This was verified by Mössbauer spectroscopy measurements, from which only Fe^{2+} could be detected in the ^{57}Fe Mössbauer spectrum.[4] To remove the remaining melt droplets from the fibre ends, the fibres were separated using a 63 mm sieve. The fibre sample F3 was commercially obtained, and produced using the spinning cup technique.[22] The raw materials were melted in an electric furnace under atmospheric conditions at about 1450 °C. Hence, the majority of iron in the resulting fibres is in the ferric state. In a previous study, the ratio $[Fe^{2+}]/[Fe_{tot}]$, where $[Fe_{tot}] = [Fe^{2+}] + [Fe^{3+}]$, was determined to be 0.35.[24] The organic binder on F3 was removed by heat-treatment in air at 450 °C for 20 min.

Table 1
Chemical compositions (in mol%) of the investigated stone wool fibre compositions F1, F2, and F3.

	SiO_2	Al_2O_3	Fe_2O_3 [a]	TiO_2	CaO	MgO	Na_2O	K_2O	Other
F1	44.7	13.5	3.3	1.3	16.1	18.7	1.7	0.6	0.1
F2	42.8	12.2	3.3	1.2	24.8	12.9	1.9	0.7	0.2
F3	47.8	16.1	2.7	0.6	18.4	3.2	6.4	4.2	0.6

[a] All iron is reported as Fe_2O_3. The ratio $[Fe^{2+}]/[Fe_{tot}]$ is ~0.35 for F3, whereas no Fe^{3+} could be detected in F1 and F2.

Sample F1 was preoxidised to study the influence of preoxidation on the crystallisation behaviour. The fibre was heat-treated at its T_g for 30 min in atmospheric air to induce oxidation of Fe^{2+} to Fe^{3+} because it has previously been shown that such a treatment of this fibre results in the formation of a 200 nm thick surface layer consisting primarily of periclase (MgO) crystals.[12] The preoxidation was performed by inserting the sample into a pre-heated electric furnace, and after 30 min, the sample was quenched by removing it from the furnace. The preoxidised F1 fibre will be termed F1-PreOx hereafter.

To study the crystallisation behaviour and HTS, the four glass fibres (F1, F1-PreOx, F2, and F3) were heat-treated in three atmospheres: argon, atmospheric air, and H_2/N_2 (1/9, v/v). The samples were inserted into a cold electric furnace, and for argon and H_2/N_2 treatments, the gas-flow was turned on. Heating and cooling of the samples were conducted at ~10 °C/min. The samples were kept at 1000 °C for 30 min.

2.2. Thermal analysis

All four types of glass fibres were thermally analyzed to study the iron oxidation and to characterize the glass transition and crystallisation processes. These analyses were conducted using a simultaneous thermal analyzer (STA, 449C Jupiter, Netzsch) by which differential scanning calorimetric (DSC) and thermogravimetric (TG) signals were simultaneously recorded. A platinum crucible containing the glass fibre sample and an empty platinum crucible were placed on the sample carrier of the STA at room temperature. Both crucibles were held 5 min at an initial temperature of 60 °C, and then heated at a rate of 10 °C/min to 1000 °C, then cooled down to 250 °C at a rate of 10 °C/min, and finally down to room temperature at a natural rate. Argon gas or atmospheric air was used as purge gas. Before measuring each sample, a baseline was recorded using two empty crucibles according to the above-stated heating procedure, which was used for correcting the DSC signal of the samples. The crucibles were covered by platinum lids during all the DSC measurements. The above-mentioned heating procedure was chosen to mimic that of the heat-treatments, but due to the use of platinum sample holder and crucibles, the thermal analysis was not conducted in the H_2/N_2 gas.

The values of the crystallisation activation energy (E_c) and the Avrami parameter n were obtained at different heating rates. The Avrami parameter is an integer number that depends on the

mechanisms of nucleation and crystal growth and the growth dimension number. The F1 fibre was measured at four different heating rates (5, 10, 20, and 30 °C/min) in air and argon. E_c was evaluated using the Kissinger equation[25]:

$$\ln\frac{T_p^2}{\alpha} = \frac{E_c}{RT_p} + \text{const}, \quad (1)$$

where T_p is the temperature of the maximum of the crystallisation peak, α is the heating rate, and R is the universal gas constant. A plot of $\ln(T_p^2/\alpha)$ versus $1/T_p$ is thus expected to be linear, and from the slope of the plot, E_c can be calculated. The Avrami parameter n can be evaluated from a single DSC experiment using Eq. (2),[26]

$$n = \frac{2.5RT_p^2}{E_c\Delta w}, \quad (2)$$

where Δw is the full width of the crystallisation peak at half maximum.

2.3. X-ray diffraction

The formed crystalline phases were determined from X-ray diffraction (XRD) measurements on the heat-treated fibres. The XRD patterns were obtained using a Siemens Bruker-AXS instrument. The fibres were placed in a drop of acetone on a platinum disk and distributed equally on the disk. After evaporation of acetone, XRD signals were recorded in the range $5° < 2\theta < 65°$ with an interval of 0.04° using Cu Kα radiation. For selected samples, the crystalline phases were quantified by adding ZnO as an internal standard.

2.4. Secondary neutral mass spectroscopy

To study the compositional changes in the surface layer that may be associated with oxidation of iron, secondary neutral mass spectroscopy (SNMS) measurements were performed on the F1, F2, and F3 fibres heat-treated in air. The measurements were performed by using an electron-gas SNMS instrument (INA 3, Leybold AG) equipped with a Balzers QMH511 quadrupole mass spectrometer and a Photonics SEM XP1600/14 amplifier. The fibres were pressed in an indium foil for fixation. A Cu mask with a 5 mm inner diameter was used to cover the sample, which was placed in a Cu sample holder, transferred into the analyzer, and sputtered using Kr plasma with an energy of ~500 eV. The time scale of the SNMS profiles was converted to a depth scale. This was done by measuring the depth of a sputtered crater on a bulk glass sample at 12 different locations using a Tencor P1 profilometer. The bulk sample had a similar composition to that of the fibres and it was measured under identical sputtering conditions. A sputter rate of 0.18 nm/s was found.

2.5. SEM imaging

To visualise the HTS of the heat-treated fibres, scanning electron microscopy (SEM) images were taken of both surfaces and cross-sections of the samples. Micrographs of the fibre surfaces were taken using an ESEM Philips XL 30 instrument, using secondary electrons for imaging. To obtain SEM images of the cross-sections of the fibres, epoxy blocks were made by casting the fibres into the epoxy. After solidification, the blocks were ground and polished using a 3 μm diamond suspension at the final step. The images of the cross-sections were recorded using a Zeiss 1540 XB SEM instrument, using both secondary electrons and backscattered electrons for imaging.

3. Results and discussion

To study the influence of the chemical composition of the as-produced fibres on the crystallisation behaviour and iron oxidation process, simultaneous thermal analyses (DSC and TG) were carried out in air and argon. Fig. 1 shows the DSC output (solid curve) and mass change (dashed curve) as a function of temperature for the F2 fibre measured in air. The mass change is calculated based on the TG measurements. The TG trace shows an increase in mass of 0.75% at temperatures above 575 °C. The increase in mass is caused by oxidation of Fe^{2+} to Fe^{3+} since oxygen is incorporated into the fibres in this process by forming metallic surface oxides.[6,7,9–12] This oxidation is connected with an exothermic peak in the DSC curve that has its maximum at ~760 °C between the glass transition temperature (T_g = 677 °C) and the onset temperature of crystallisation (T_c = 865 °C). The inflection point of the TG curve corresponds to the maximum of the oxidation peak.

Table 2 contains the T_g, T_c, and T_p values determined in both argon and air of the as-produced F1, F2, and F3 fibres and the preoxidised F1 fibre. The F3 fibre has the lowest value of T_g in both atmospheres due to the relatively high content of alkali oxides (Na_2O and K_2O) in these fibres (see Table 1). Addition of alkali oxides to silica glass is well known to cause a decrease of T_g.[27] In general, the crystallisation begins at a lower temperature when the fibres F1, F1-PreOx, and F2 are heated in air than when they are heated in argon (Table 2). During the upscanning in air, oxidation of Fe^{2+} takes place in these fibres, which leads to the formation of a nano-crystalline surface layer. This layer is not

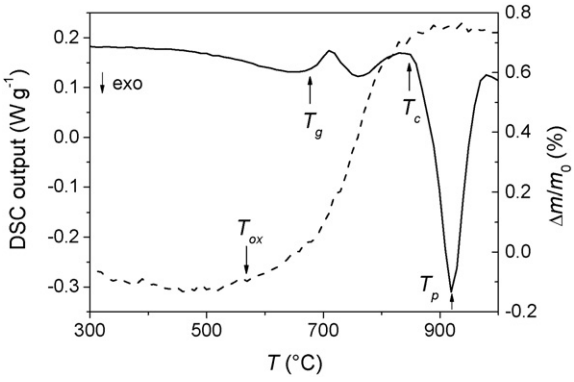

Fig. 1. Solid curve: the DSC output of the as-produced F2 fibre as a function of temperature (T) in air at a heating rate of 10 °C/min. T_{ox} is the onset temperature of the oxidation; T_g the glass transition temperature; T_c the onset temperature of crystallisation; and T_p the peak temperature of crystallisation. Dashed curve: the corresponding normalised mass change $\Delta m/m_0$, where Δm and m_0 are the mass change and the initial mass of the sample, respectively.

Table 2
T_g, T_c, and T_p of the as-produced F1, F2, and F3 fibres and the F1 fibre preoxidised at T_g for 30 min. The characteristic temperatures were determined from DSC measurements performed at an upscanning rate of 10 °C/min under an atmosphere of air or argon.

	Atmosphere	T_g (°C)	T_c (°C)	T_p (°C)
F1	Argon	681	871	885
	Air	678	864	917
F1-PreOx	Argon	685	835	867
	Air	687	822	883
F2	Argon	675	871	917
	Air	677	865	920
F3	Argon	664	837	868
	Air	659	837	880

Table 3
Effect of heating rate (α) on the peak crystallisation temperature (T_p) of the as-produced F1 fibres. T_p was determined from DSC measurements performed under an atmosphere of argon or air. From the variation of T_p with α, the activation energy of crystallisation (E_c) and the average value of the Avrami parameter (n_{avg}) are determined by using Eqs. (1) and (2), respectively.

Atmosphere	α (°C/min)	T_p (°C)	E_c (kJ/mol)	n_{avg}
Argon	5	861	338 ± 15	4.9 ± 0.2
	10	885		
	20	906		
	30	917		
Air	5	891	260 ± 9	1.9 ± 0.1
	10	917		
	20	947		
	30	968		

created during heating in argon since no oxidation occurs in this case (Fig. 2). In comparison to F1 and F2, only limited (∼0.1% mass increase) oxidation of iron occurs in the F3 fibre heated in air and for this fibre, T_c is the same in both atmospheres. This is explained by a lower initial $[Fe^{2+}]/[Fe_{tot}]$ ratio of F3 compared to that of F1 and F2. The preoxidised F1 fibre has a lower T_c than the as-produced F1 fibre in both atmospheres.

These observations indicate that the nano-crystalline layer lowers the activation energy for crystallisation (E_c). The reason for this is that the nuclei more easily grow from the existing crystalline surface layer of the fibres heat-treated in air than from the amorphous surface of the fibres heat-treated in argon. The surface nucleation of the fibres is a typical heterogeneous nucleation that has lower activation energy than the homogeneous nucleation. This is confirmed by the fact that the dependence of T_p on the heating rate for the F1 fibre heated in air is stronger than that in argon. From these DSC data, E_c and the Avrami parameter n can be calculated using Eqs. (1) and (2), respectively. The calculated values are given in Table 3 and it is found that E_c of the air-treated F1 fibre is indeed lower than that of the

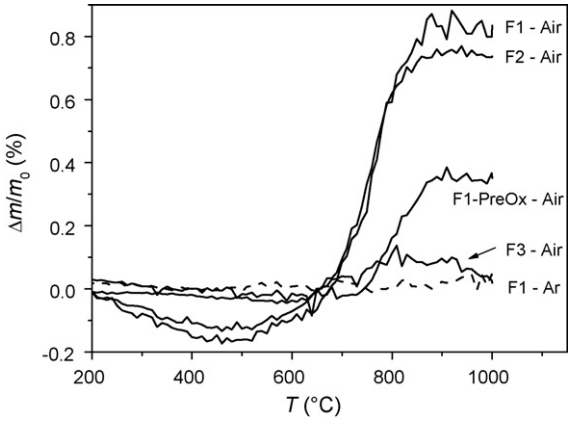

Fig. 2. Normalised mass change $\Delta m/m_0$, where Δm and m_0 are the mass change and the initial mass of the sample, respectively, of the F1, F1-PreOx, F2, and F3 fibres as a function of temperature (T). The mass change was measured at an upscanning rate of 10 °C/min in air (solid curves). The mass change was also measured in argon for the F1 fibre (dashed curve). For reasons of clarity, the curves for F1-PreOx, F2, and F3 in argon are not shown, but they appear similar to that of F1.

argon-treated F1 fibre. The Avrami parameter changes from ∼5 for the argon-treated fibre to ∼2 for the air-treated fibre. One-dimensional crystal growth should give $n = 1$, two-dimensional $n = 2$, and three-dimensional $n \geq 3$. n-values of 1–2 correspond to surface crystallisation.[28,29] Hence, the oxidation of iron that takes place during upscanning in air leads to formation of a nano-crystalline layer (dominantly MgO) at the surface, and these crystals lower the energy barrier of surface nucleation, i.e., nucleation in the interface between the nanolayer and the glassy bulk part of the fibres. The presence of nuclei is a prerequisite for crystal growth.[27] For the fibres studied here, the surface nucleation and the subsequent crystal growth (towards the interior of the fibres) are more intense, easier and faster than crystallisation in the interior of the fibres due to significantly higher specific surfaces of the fibres compared to normal bulk glasses. In other words, the surface crystallisation dominates the overall crystallisation of the fibres.[30] That is the reason why the onset temperature of crystallisation should be attributed to surface crystallisation (mainly crystal growth).

To reveal to which extent the nano-crystalline surface layer is created during heat-treatment in air, secondary neutral mass spectroscopy (SNMS) is employed to determine the concentration depth profiles of the F1, F2, and F3 fibres that, prior to the measurements, have been heat-treated in air. Fig. 3a shows the normalised concentration depth profiles of five elements (Mg, Fe, Ca, Si, and O) of the F1 fibre. Only five elements are shown in the figure to allow for a better comparison. A high surface concentration of magnesium and iron is observed, which is due to the outward diffusion of these ions. Hence, the nano-crystalline surface layer is indeed created during heating in air (in the temperature range from ∼575 to 850 °C, see Fig. 2) and it is still present after the treatment at 1000 °C for 30 min (see Fig. 3a), i.e., it is present after the bulk crystallisation process has been completed. The diffusion of Fe^{2+} has previously been observed,[7,9,12] which resulted in the formation of a Fe_2O_3-containing surface layer during oxidation. No outward diffusion of Ca^{2+} is observed, which can be explained by the smaller size of Mg^{2+} and Fe^{2+} compared to Ca^{2+}.[12] The low surface concentration of calcium and silicon is due to the enrichment of magnesium and iron near the surface.

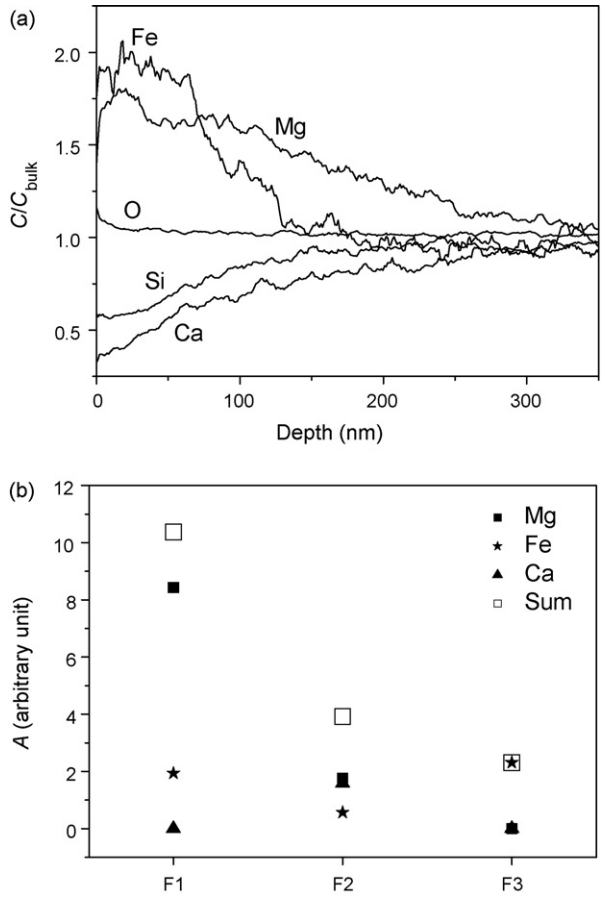

Fig. 3. (a) Concentration depth profiles of different elements in the F1 fibre heat-treated in air at 1000 °C for 30 min. C/C_{bulk} is the ratio of the concentration of a given element at a given depth to the average concentration of that element in the bulk of the sample. (b) The SNMS peak areas (A) of Mg, Ca, and Fe and their sum for the F1, F2, and F3 fibres heat-treated in air at 1000 °C for 30 min. The areas are calculated between the SNMS concentration curves of Mg, Ca, and Fe and the horizontal line through $C = C_{bulk}$ when enrichment of the ion near the surface occurs. The area is set equal to zero if no enrichment occurs.

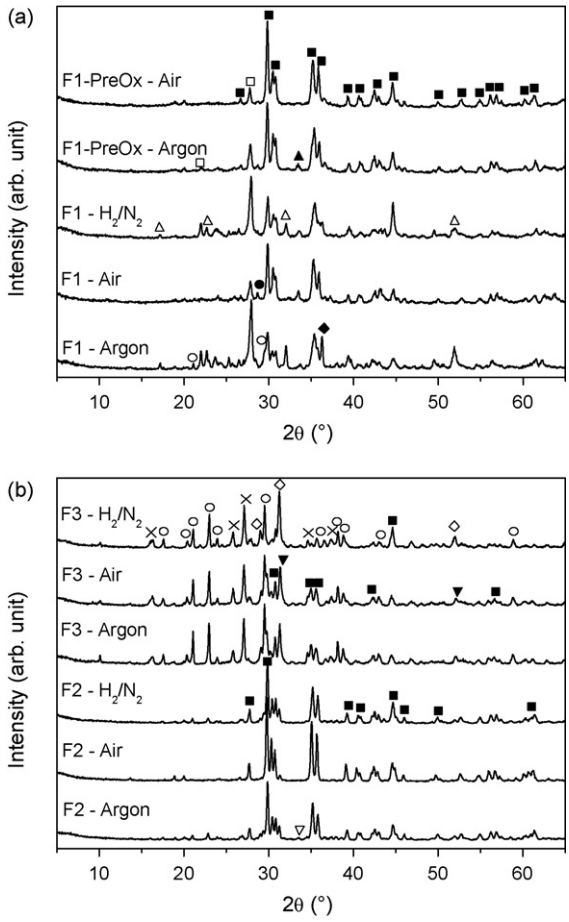

Fig. 4. X-ray diffraction patterns for the fibres heat-treated at 1000 °C for 30 min under various atmospheres. The peaks have been assigned to augite (■), anorthite (□), andradite (▲), forsterite (△), albite (●), nepheline (◯), olivine (♦), akermanite (◊), leucite (×), gehlenite (▼), and grossular (▽).

In Fig. 3b, the peak areas of the Mg, Ca, and Fe curves are shown for the F1, F2, and F3 fibres heated in air. The areas are calculated between the SNMS concentration curves of Mg, Ca, and Fe and the horizontal line through $C = C_{bulk}$ when enrichment of the element occurs near the surface. In addition, the sum of the areas of Mg, Ca, and Fe for each type of fibre is shown. In the F2 fibre, diffusion of magnesium, iron, and calcium occurs to approximately the same extent, whereas in the F1 fibre, diffusion of magnesium is predominant. Fig. 3b shows that the sum of the areas for F2 is smaller than that for F1. This is probably due to the higher CaO concentration in F2 than in F1 (see Table 1), i.e., F2 contains a high content of the relatively slow Ca^{2+} ions. Only outward diffusion of iron occurs in F3 and it occurs to a relatively small extent. This is due to the small degree of iron oxidation in this fibre (Fig. 2). In summary, the SNMS measurements reveal that the thickness of the layer increases with increasing concentration of Fe^{2+} and Mg^{2+} in the as-prepared fibres.

To identify the crystalline phases formed in the heat-treated fibres, XRD measurements were performed on the F1, F1-PreOx, F2, and F3 fibres heat-treated in the three types of atmospheres (Fig. 4). Previous studies have shown that these fibres are fully amorphous before the heat-treatments.[2,12,30] In Table 4, the identified crystal phases are shown, and for some of the samples, the degree of crystallisation (D_c) determined by XRD is also shown. Four statements can be made based on the XRD data. First, the identity of the formed crystalline phases depends on the chemical composition of the fibres. For instance, the alkali-rich F3 fibre contains the alkali-bearing nepheline and leucite as the main crystalline phases, whereas F1 and F2 contain other types of main crystalline phases. Second, the atmosphere does not have an influence on the identity of the formed bulk crystalline phases. In other words, the oxidation of iron does not have a major impact on the crystal identity even though the nano-crystalline surface layer lowers the onset temperature of crystallisation as discussed above. Third, the highest D_c is achieved by heat-treating F3, which contains the highest content of alkali oxides, and hence, possesses the lowest T_g. Therefore, the required diffusion for the bulk crystallisation process can proceed relatively fast. Fourth, preoxidation considerably lowers D_c. Oxidation leads to an increase of viscosity due to the conversion of network-modifying Fe^{2+} ions to network-forming Fe^{3+} ions[31,32] and the outward diffusion of network-modifying

Table 4
Crystal phases in the F1, F1-PreOx, F2, and F3 fibres heat-treated under different atmospheres at 1000 °C for 30 min. The crystal phases were identified from XRD measurements (see Fig. 4). For some samples, the degree of crystallisation (D_c) after heat-treatment was determined.

	Atmosphere	Main phase(s)	Minor phase(s)	D_c (wt%)
F1	Argon	Au/Fo/An	Al/Ne/Ol	85.4
	Air	Au/And/An	Al	84.8
	H_2/N_2	An	Au/And/Fo	–
F1-PreOx	Argon	Au	And/An	66.0
	Air	Au	An	59.7
F2	Argon	Au/Ne	Ake/Gr	–
	Air	Au		84.6
	H_2/N_2	Au/Geh	Ne	–
F3	Argon	Ne/Leu	Au/Ake	–
	Air	Ne/Au	Geh/Leu	96.9
	H_2/N_2	Ne/Leu	Ake/Au	–

Au = augite [$Ca(Mg,Fe,Al)(Si,Al)_2O_6$], Fo = forsterite [Mg_2SiO_4], Ne = nepheline [$(Na,K)AlSiO_4$], Ol = olivine [$(Mg,Fe)_2SiO_4$], An = anorthite [$CaAl_2Si_2O_8$], Al = albite [$NaAlSi_3O_8$], And = andradite [$Ca_3Fe_2(SiO_4)_3$], Leu = leucite [$KAlSi_2O_6$], Geh = gehlenite [$Ca_2Al(AlSi)O_7$], Ake = akermanite [$Ca_2MgSi_2O_7$], and Gr = grossular [$Ca_3Al_2(SiO_4)_3$].

cations. As a result, the polymerisation degree of the structural network, and hence, the viscosity in the interior of the fibres increases. This in turn lowers ionic mobilities that are required for crystallisation. Thus, crystallisation in the interior of the fibres is suppressed, while the surface nucleation and the subsequent inward crystal growth from the surface layer are enhanced.[13,33]

The HTS of the fibres is visualised from SEM images of surfaces and cross-sections of the fibres. For comparison, the untreated F1 is shown in Fig. 5 to illustrate the original geometric shape of the fibres at room temperature. The untreated F2 and F3 fibres appear similar. Fig. 6 shows SEM images of

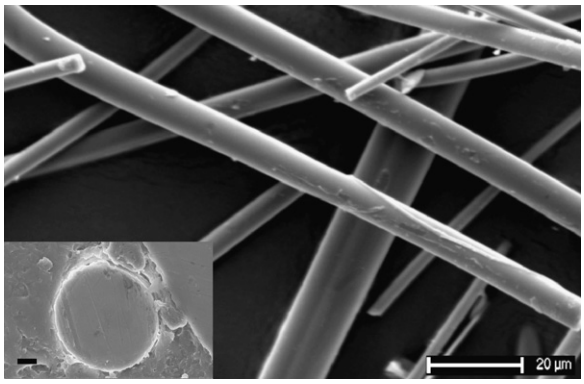

Fig. 5. SEM surface image of the as-produced F1 fibre. Inset: SEM image of a cross-section of the same fibre recorded by secondary electrons detector. Scale bar corresponds to 1 μm.

the fibres heat-treated in air. The F1 and F2 fibres are capable of maintaining their original geometry to a large extent. In contrast, the F3 fibres are broken into minor pieces, even though the fibres still possess circumferential surfaces. An oxide surface nanolayer is created during heating of F1, F2, and F3 in air, but the extent of the layer formation is smallest for F3 (Fig. 3b). XRD measurements have revealed the crystalline nature of the oxide surface layer.[12] The following explanations could account for the origin of the HTS created by the nano-crystalline layer.[12] First, MgO and CaO are highly refractory since they possess bulk melting points (T_m) of approximately 2980 and 2615 °C, respectively.[34,35] Even though T_m decreases with decreasing crystal size for crystals,[36] the melting point of the nano-crystalline layer should be high enough to sustain the heating process below T_c. In addition, it should be noticed that MgO crystals may be mixed with CaO crystals when Mg^{2+} and Ca^{2+} diffuse simultaneously. This eutectic effect can also lower T_m. Second, the increase of viscosity that is accompa-

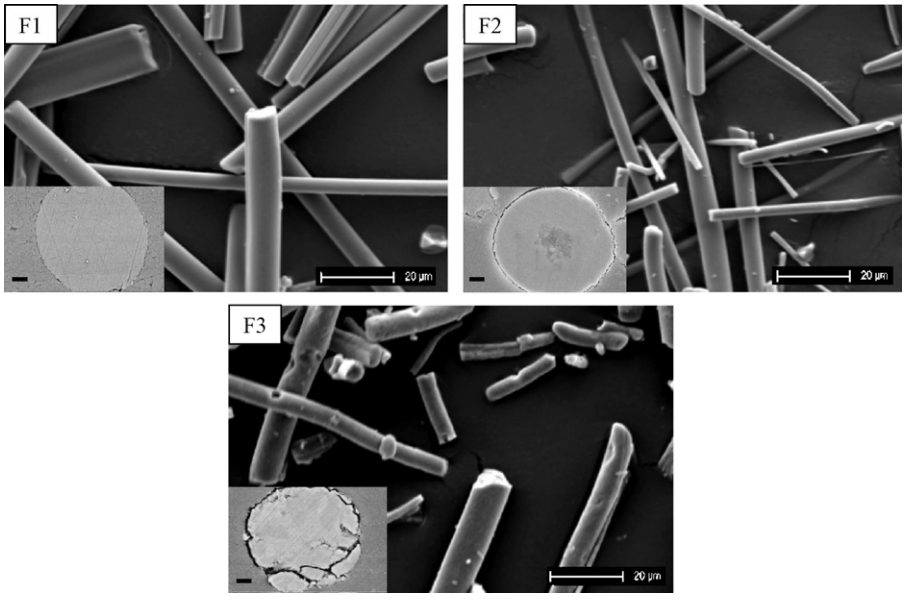

Fig. 6. SEM surface images of the F1, F2, and F3 fibres heat-treated in air at 1000 °C for 30 min. Insets: SEM images of cross-sections of the same fibres. Scale bar corresponds to 1 μm. All cross-section images were recorded by backscattered electrons detector.

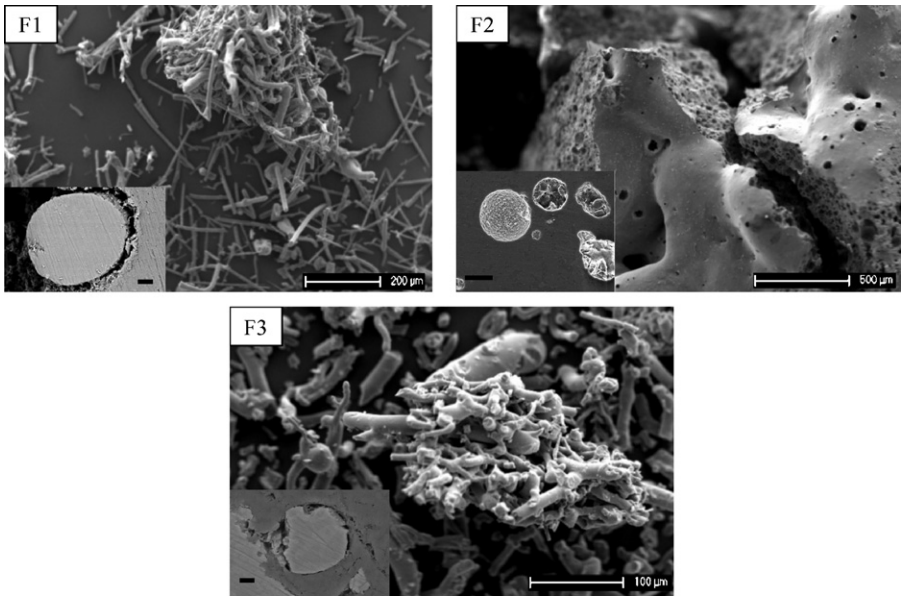

Fig. 7. SEM surface images of the F1, F2, and F3 fibres heat-treated in argon at 1000 °C for 30 min. Insets: SEM images of cross-sections of the same fibres. Scale bar corresponds to 1 μm for F1 and F3 and 5 μm for F2. Cross-section images of F1 and F3 were recorded by backscattered electrons detector, whereas F2 was recorded by secondary electrons detector.

nied by iron oxidation decreases the deformation degree of the fibres.

When the F1, F2, and F3 fibres are heat-treated in argon (Fig. 7) and H_2/N_2 (Fig. 8), they partly lose their shape and are sintered into crystalline aggregates. Sintering does not occur in the F1 fibre that has been preoxidised and subsequently heat-treated in argon due to the MgO nanocrystals.[12] The F1 fibres seem to have the best HTS in argon and H_2/N_2 since these fibres retain their circumferential surfaces to some extent. F1 has a relatively high content of MgO, indicating that the HTS of SWFs can be improved by increasing the MgO content. In the temperature range between T_g and T_c, the fibres are viscous liquids and they will gradually lose their structure with increasing temperature. Mg^{2+} has relatively high field strength due to its small size and it therefore strongly attracts the nearby oxygen anions. This means that Mg^{2+} ions are capable of preventing the gradual deformation with increasing temperature to a larger extent than, e.g., Ca^{2+} and Na^{+} ions as they have lower field strength.

The SEM images show that both the heat-treatment atmosphere and the fibre composition affect the HTS. The composition also affects the crystallisation behaviour and the

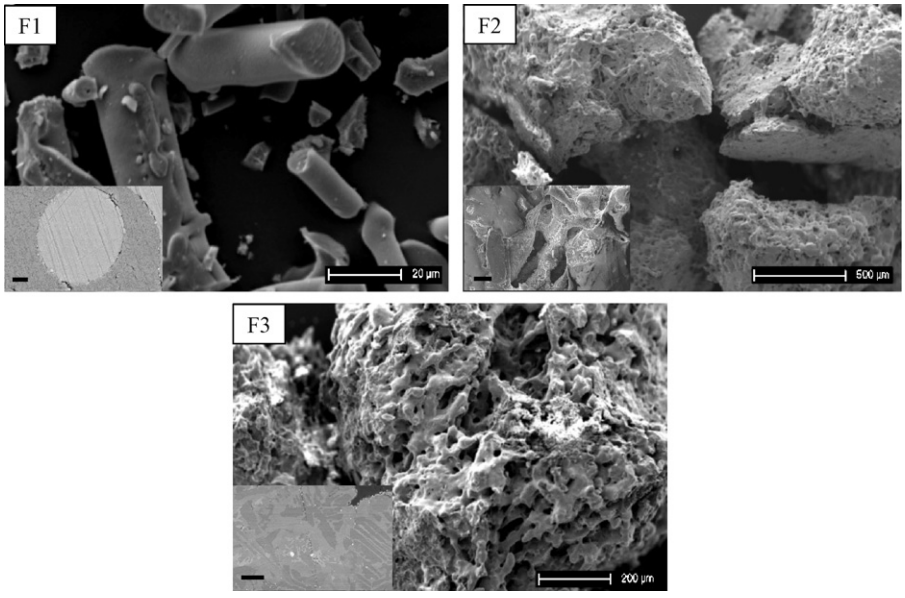

Fig. 8. SEM surface images of the F1, F2, and F3 fibres heat-treated in H_2/N_2 at 1000 °C for 30 min. Insets: SEM images of cross-sections of the same fibres. Scale bar corresponds to 1 μm for F1, 20 μm for F2, and 5 μm for F3. Cross-section images of F1 and F3 were recorded by backscattered electrons detector, whereas F2 was recorded by secondary electrons detector.

atmosphere has an effect on the crystallisation onset and peak temperatures. In contrast, the atmosphere has no impact on the type of crystalline phases. Therefore, it can be inferred that the identity of the crystalline phases does not influence the HTS.

4. Conclusions

Oxidation of Fe^{2+} to Fe^{3+} in alumino-silicate glass fibres enhances the HTS of the fibres in atmospheric air. This is due to the formation of a nano-crystalline surface layer and the increase of viscosity as a result of the oxidation. The layer is maintained after the bulk crystallisation process has been completed. With an increasing initial content of Fe^{2+} and Mg^{2+} in the fibres, the thickness of the layer increases. The HTS of the fibres is lower in argon and H_2/N_2 atmospheres than in atmospheric air. This is due to the fact that the fibres heat-treated in argon and H_2/N_2 atmospheres lack the nano-crystalline surface layer that lowers the onset temperature, Avrami parameter, and activation energy of the crystallisation, and thereby protect the fibres from sintering. Different types of crystalline phases form during iso-thermal heating of the fibres at 1000 °C, but it is inferred that the identity of the crystalline phases does not affect the HTS.

Acknowledgements

The authors thank T.T. Mikkelsen, J.S. Nielsen, and P.M. Rosenkjær for conducting heat-treatments and M. Zellmann and T. Peter for performing XRD and SNMS measurements, respectively. They thank W. Krøis and J. Rafaelsen for experimental assistance with SEM imaging. They also thank M. Jensen, J. Deubener, and D. Lybye for useful discussions. This work was financially supported by Rockwool International A/S.

References

1. Širok B, Blagojević B, Bullen P. *Mineral wool*. Cambridge: Woodhead Publishing; 2008.
2. Kirkegaard LF, Korsgaard M. *Impact of redox state and pre-oxidation on diffusion, crystallisation, and high temperature behaviour of iron containing alumino-silicate glass fibres*. Master Thesis. Denmark: Aalborg University; 2004.
3. Kaasgaard M, Jacobsen PAL, Yue YZ. Influence of oxygen partial pressure on crystallization behavior and high-temperature stability of stone wool fibres. *Glass Sci Technol* 2005;**78**:63–8.
4. Kirkegaard LF, Korsgaard M, Yue YZ. Redox behavior of iron bearing glass fibers during heat treatment under atmospheric conditions. *Glass Sci Technol* 2005;**78**:1–6.
5. Yue YZ, Korsgaard M, Kirkegaard LF, Heide G. Oxidation diffusion process in the ferrous iron-bearing glass fibers near glass temperature. In: *Proceedings of XX international congress on glass*. 2004. p. 1–6.
6. Cook GB, Cooper RF, Wu T. Chemical diffusion and crystalline nucleation during oxidation of ferrous iron-bearing magnesium aluminosilicate glass. *J Non-Cryst Solids* 1990;**120**:207–22.
7. Cooper RF, Fanselow JB, Poker DB. The mechanism of oxidation of a basaltic glass: chemical diffusion of network-modifying cations. *Geochim Cosmochim Acta* 1996;**60**:3253–65.
8. Cooper RF, Fanselow JB, Weber JKR, Merkley DR, Poker DB. Dynamics of oxidation of a Fe^{2+}-bearing aluminosilicate (basaltic) melt. *Science* 1996;**274**:1173–6.
9. Smith DR, Cooper RF. Dynamic oxidation of a Fe^{2+}-bearing calcium–magnesium–aluminosilicate glass: the effect of molecular structure on chemical diffusion and reaction morphology. *J Non-Cryst Solids* 2000;**278**:145–63.
10. Cook GB, Cooper RF. Iron concentration and the physical processes of dynamic oxidation in an alkaline earth aluminosilicate glass. *Am Miner* 2000;**85**:397–406.
11. Burkhard DJM. Crystallization and oxidation of Kilauea basalt glass: processes during reheating experiments. *J Petrol* 2001;**42**:507–27.
12. Yue YZ, Korsgaard M, Kirkegaard LF, Heide G. Formation of nanocrystalline layer on the surface of stone wool fibers. *J Am Ceram Soc* 2009;**92**:62–7.
13. Karamanov A, Pisciella P, Pelino M. The crystallisation kinetics of iron rich glass in different atmospheres. *J Eur Ceram Soc* 2000;**20**:2233–7.
14. Sørensen PM, Pind M, Yue YZ, Nielsen ER, Rawlings RD, Boccaccini AR. Effect of the redox state and concentration of iron on the crystallization behavior of iron-rich aluminosilicate glasses. *J Non-Cryst Solids* 2005;**351**:1246–53.
15. Karamanov A, Pisciella P, Cantalini C, Pelino M. Influence of Fe^{3+}/Fe^{2+} ratio on the crystallization of iron-rich glasses made with industrial wastes. *J Am Ceram Soc* 2000;**83**:3153–7.
16. Lonnroth N, Yue YZ. Structural order and crystallization of an iron-rich aluminosilicate liquid under oxidizing condition. *J Non-Cryst Solids* 2008;**354**:1190–3.
17. Tosic MB, Dimitrijevic RZ, Radosavlievic SA, Duricic MA. Influence of the iron oxidation state on the nucleation of basalt glass. *J Serb Chem Soc* 1998;**63**:1019–30.
18. Burkhard DJM, Scherer T. The effect of initial oxidation state on crystallization of basaltic glass. *J Non-Cryst Solids* 2006;**352**:3961–9.
19. Yang HZ, Chen CP, Sun HW, Liu HX, Hu X. Influence of heat-treatment schedule on crystallization and microstructure of bauxite tailing glass–ceramics coated on tiles. *J Mater Process Technol* 2008;**197**:206–11.
20. Žnidaršič-Pongrac V, Kolar D. The crystallization of diabase glass. *J Mater Sci* 1991;**26**:2490–4.
21. Lund MD, Yue YZ. Influences of chemical aging on the surface morphology and crystallization behavior of basaltic glass fibers. *J Non-Cryst Solids* 2008;**354**:1151–4.
22. Axten CW, Bauer JF, Boymel PM, Copham JD, Cunningham RN, Kamstrup O, et al. Fiber forming processes for MMVF. In: Easters W, editor. *Man-made vitreous fibers: nomenclature, chemistry and physical properties*. OH: TIMA Inc.; 1991–1993. p. 17.
23. Yue YZ, von der Ohe R, Jensen SL. Fictive temperature, cooling rate, and viscosity of glasses. *J Chem Phys* 2004;**120**:8053–9.
24. Nielsen ER, Augustesen M, Stahl K. Devitrification and high temperature properties of mineral wool. *Mater Sci Forum* 2007;**558–559**:1255–60.
25. Kissinger HE. Reaction kinetics in differential thermal analysis. *Anal Chem* 1957;**29**:1702–6.
26. Augis JA, Bennett JE. Calculation of the Avrami parameters for heterogeneous solid state reactions using a modification of the Kissinger method. *J Therm Anal* 1978;**13**:283–92.
27. Shelby JE. *Introduction to Glass Science and Technology*. Cambridge: The Royal Society of Chemistry; 2005.
28. Matusita K, Sakka S. Kinetic study on crystallization of glass by differential thermal analysis—criterion on application of Kissinger plot. *J Non-Cryst Solids* 1980;**38–39**:741–6.
29. Marotta A, Buri A, Branda F. Surface and bulk crystallization in non-isothermal devitrification of glasses. *Thermochim Acta* 1980;**40**:397–403.
30. Moesgaard M, Pedersen HD, Yue YZ, Nielsen ER. Crystallization in stone wool fibres. *J Non-Cryst Solids* 2007;**353**:1101–8.
31. Mysen BO, Seifert F, Virgo D. Structure and redox equilibria of iron-bearing silicate melts. *Am Miner* 1980;**65**:867–84.
32. Dyar MD. A review of Mössbauer data on inorganic glasses: the effects of composition on iron valency and coordination. *Am Miner* 1985;**70**:304–16.

33. Karamanov A, Taglieri G, Pelino M. Sintering in nitrogen atmosphere of iron-rich glass–ceramics. *J Am Ceram Soc* 2004;**87**:1354–7.
34. Ronchi C, Sheindlin M. Melting point of MgO. *J Appl Phys* 2001;**90**:3325–31.
35. Lide DR. *CRC handbook of chemistry and physics*. London: CRC Press; 2006.
36. Gersten JI, Smith FW. *The physics and chemistry of materials*. New York: John Wiley & Sons, Inc.; 2001.